
Invertible Gaussian Reparameterization: Revisiting the Gumbel-Softmax

Andrés Potapczynski
Columbia University
ap3635@columbia.edu

Gabriel Loaiza-Ganem¹
Layer 6 AI
gabriel@layer6.ai

John P. Cunningham
Columbia University
jpc2181@columbia.edu

Abstract

The Gumbel-Softmax is a continuous distribution over the simplex that is often used as a relaxation of discrete distributions. Because it can be readily interpreted and easily reparameterized, the Gumbel-Softmax enjoys widespread use. We show that this relaxation experiences two shortcomings that affect its performance, namely: numerical instability caused by its temperature hyperparameter and noisy \mathbb{KL} estimates. The first requires the temperature values to be set too high, creating a poor correspondence between continuous components and their respective discrete complements. The second, which is of fundamental importance to variational autoencoders, severely hurts performance. We propose a flexible and reparameterizable family of distributions that circumvents these issues by transforming Gaussian noise into one-hot approximations through an invertible function. Our construction improves numerical stability, and outperforms the Gumbel-Softmax in a variety of experiments while generating samples that are closer to their discrete counterparts and achieving lower-variance gradients. Furthermore, with a careful choice of the invertible function we extend the reparameterization trick to distributions with countably infinite support.

1 Introduction

Numerous machine learning tasks involve optimization problems over discrete stochastic components whose

parameters we wish to learn. Mixture and mixed-membership models, variational autoencoders, language models and reinforcement learning fall into this category (Johnson et al., 2016; Kingma and Welling, 2014; Kusner and Hernández-Lobato, 2016; Glynn, 1990). Ideally, as with fully continuous models, we could use stochastic optimization via backpropagation. One strategy to compute the necessary gradients is using score estimators (Glynn, 1990; Williams, 1992), however these estimates suffer from high variance which leads to slow convergence, despite some efforts (Miller et al., 2017). Another strategy is to find a reparameterizable continuous relaxation of the discrete distribution. Reparameterization gradients exhibit lower variance but are contingent on finding such a relaxation. Jang et al. (2017) and Maddison et al. (2017) independently found such a continuous relaxation via the Gumbel-Softmax (GS) or Concrete distribution.

The GS has experienced wide use and has been extended to other settings, such as permutations (Linderman et al., 2018), subsets (Xie and Ermon, 2019) and more (Balog et al., 2017). Its success relies on several qualities that make it appealing: *(i)* it is reparameterizable, that is, it can be sampled by transforming parameter-independent noise through a smooth function, *(ii)* it can approximate (i.e. converge in distribution to) any discrete distribution on the vertices, *(iii)* it has a closed form density, and *(iv)* its parameters can be interpreted as the discrete distribution that it is relaxing. While the last quality is mathematically pleasing, it is not a necessary condition for a valid relaxation. Here we ask: *how important is this parameter interpretability?* In the context of deep learning models, interpreting the parameters is not a first concern, and we show that the GS can be significantly improved upon by giving up this quality.

In spite of its qualities, we show that the GS has two shortcomings that we aim to amend: the first one is that using low temperature hyperparameters causes numerical instabilities, which we explain mathemat-

Submitted to AISTATS 2020.

¹ Work partially done while at Columbia University.

ically in section 3. The second shortcoming is that when the optimization objective involves a \mathbb{KL} divergence, it has to be noisily estimated with a Monte Carlo approach, which is not the case in the continuous setting as the \mathbb{KL} can usually be evaluated in closed form (Kingma and Welling, 2014). This shortcoming is particularly relevant for variational autoencoders (Kingma and Welling, 2014). In this paper we propose an alternative family of distributions over the simplex to achieve this relaxation, which we call Invertible Gaussian Reparameterization (IGR). Our reparameterization works by transforming Gaussian noise through an invertible transformation onto the simplex, and a temperature hyperparameter allows the distribution to concentrate its mass around the vertices. We show that our distribution addresses both shortcomings of the GS, results in relaxations that match their discrete counterparts better, and empirically outperforms the GS.

The contributions of our paper are (i) highlighting two shortcomings of the GS, (ii) introducing the IGR family of distributions over the simplex to address these shortcomings, and (iii) showing that the interpretability of the parameters of the GS does not translate into better performance and that IGR outperforms the GS in a variety of experiments. Our code is available at <https://github.com/cunningham-lab/igr>.

2 Background

2.1 The reparameterization trick

Many problems in machine learning can be formulated as an optimization program over an expectation:

$$\phi^* = \arg \max_{\phi} L(\phi) := \arg \max_{\phi} \mathbb{E}_{z \sim q_{\phi}} [f(z)] \quad (1)$$

where q_{ϕ} is a distribution over \mathcal{S} parameterized by ϕ and $f : \mathcal{S} \rightarrow \mathbb{R}$. In order to use stochastic gradient methods (Robbins and Monro, 1951; Bottou, 2012), the gradient of L has to be estimated. A first option is to use score estimators (Glynn, 1990; Williams, 1992):

$$\nabla_{\phi} L(\phi) \approx \frac{1}{B} \sum_{b=1}^B f(z_b) \nabla_{\phi} \log q_{\phi}(z_b) \quad (2)$$

where $z_1, \dots, z_B \sim q_{\phi}$. In practice score estimators usually exhibit high variance (Miller et al., 2017). The reparameterization trick (Kingma and Welling, 2014) provides an alternative estimate of this gradient which empirically has less variance, resulting in more efficient optimization. The reparameterization trick consists of finding a function $g(\epsilon, \phi)$ such that g is differentiable with respect to ϕ and if $z \sim q_{\phi}$, then:

$$z \stackrel{d}{=} g(\epsilon, \phi) \quad (3)$$

where ϵ is a continuous random variable whose distribution does not depend on ϕ . The gradient is then estimated by:

$$\nabla_{\phi} L(\phi) \approx \frac{1}{B} \sum_{b=1}^B \nabla_{\phi} f(g(\epsilon_b, \phi)) \quad (4)$$

where $\epsilon_1, \dots, \epsilon_B$ are iid samples from the distribution of ϵ . For example, if $\phi = (\mu, \sigma)$ and $q_{\phi} = \mathcal{N}(\mu, \sigma^2)$ then the reparameterization trick is given by $g(\epsilon, \phi) = \mu + \sigma\epsilon$ with $\epsilon \sim \mathcal{N}(0, 1)$.

2.2 Continuous relaxations

While we can use the score estimator of equation 2 whether q_{ϕ} has continuous or discrete support, the reparameterization gradient of equation 4 is only valid when q_{ϕ} has continuous support. To extend the reparameterization trick to the discrete setting, thus avoiding the high variance issues of score estimators, suppose q_{ϕ} is a distribution over the set $\mathcal{S} = \{1, 2, \dots, K\}$. We use one-hot representations of length K for the elements of \mathcal{S} , so that \mathcal{S} can be interpreted as the vertices of the $(K-1)$ -simplex, $\Delta^{(K-1)} = \{z \in \mathbb{R}^K : z_k \geq 0 \text{ and } \sum_{k=1}^K z_k = 1\}$. The idea is to now place a distribution over $\Delta^{(K-1)}$ that approximates q_{ϕ} . Note that placing a distribution over $\Delta^{(K-1)}$ is equivalent to placing a distribution over $\mathcal{S}^{(K-1)} = \{z \in \mathbb{R}^{K-1} : z_k \geq 0 \text{ and } \sum_{k=1}^{K-1} z_k \leq 1\}$, as the last coordinate can be obtained from the previous ones: $z_K = 1 - \sum_{k=1}^{K-1} z_k$. Placing a distribution over $\mathcal{S}^{(K-1)}$ is mathematically convenient as $\mathcal{S}^{(K-1)} \subset \mathbb{R}^{K-1}$ has positive Lebesgue measure, while $\Delta^{(K-1)} \subset \mathbb{R}^K$ does not. Although this distinction might appear as an irrelevant technicality, it allows to correctly compute our Jacobians in section 4. The optimization problem of equation 1 is then relaxed to:

$$\tilde{\phi}^* = \arg \max_{\tilde{\phi}} \tilde{L}(\tilde{\phi}) := \arg \max_{\tilde{\phi}} \mathbb{E}_{\tilde{z} \sim \tilde{q}_{\tilde{\phi}}} [\tilde{f}(\tilde{z})] \quad (5)$$

where $\tilde{q}_{\tilde{\phi}}$ is a distribution over $\mathcal{S}^{(K-1)}$ and the function $\tilde{f} : \mathcal{S}^{(K-1)} \rightarrow \mathbb{R}$ is a relaxation of f to $\mathcal{S}^{(K-1)}$. As long as $\tilde{q}_{\tilde{\phi}}$ concentrates most of its mass around \mathcal{S} and \tilde{f} is smooth, this relaxation is sensible. If $\tilde{q}_{\tilde{\phi}}$ can be reparameterized as in equation 3, then we can use the reparameterization trick. We make two important notes: first, not only the distribution is relaxed, the function f also has to be relaxed to \tilde{f} because it now needs to take inputs in $\mathcal{S}^{(K-1)}$ and not just \mathcal{S} . In other words, not only the distribution has to be relaxed, the objective does too. While extending f to \tilde{f} can often be straightforward, it is not always the case. This point is an important but often overlooked technicality, which is particularly relevant for variational

autoencoders as we will see later. Second, the parameters $\tilde{\phi}$ of the relaxed distribution need not match the parameters ϕ of the original distribution.

Maddison et al. (2017) and Jang et al. (2017) proposed the Gumbel-Softmax distribution, which is parameterized by $\alpha \in (0, \infty)^K$ and a temperature hyperparameter $\tau \in (0, \infty)$, and can be reparameterized as follows:

$$\tilde{z} \stackrel{d}{=} \text{softmax}((\epsilon + \log \alpha)/\tau) \quad (6)$$

where $\epsilon \in (0, \infty)^K$ is a vector with independent Gumbel(0, 1) entries and log refers to elementwise logarithm. Note that when the temperature approaches 0, not only does the GS concentrate its mass around \mathcal{S} , but it converges to a distribution proportional to α . The GS distribution implied by equation 6 can be shown to be:

$$\tilde{q}_{\alpha, \tau}(\tilde{z}) = (K-1)! \tau^{K-1} \prod_{k=1}^K \left(\frac{\alpha_k \tilde{z}_k^{-\tau-1}}{\sum_{k=1}^K \alpha_k \tilde{z}_k^{-\tau}} \right) \quad (7)$$

We highlight the difference between α and $\tilde{\phi}$: the former is the parameter of the GS distribution and might depend on the latter, which is the parameter with respect to which we optimize in equation 5. For example, α might be the output of a neural network parameterized by $\tilde{\phi}$. As we will see in section 2.3, a common use of the GS is to relax objectives of the form:

$$\mathbb{KL}(q_\phi || p_0) = \mathbb{E}_{z \sim q_\phi} \left[\log \frac{q_\phi(z)}{p_0(z)} \right] \quad (8)$$

where p_0 is a distribution over \mathcal{S} . Relaxing this \mathbb{KL} requires additional care: it cannot be relaxed to $\mathbb{KL}(\tilde{q}_{\tilde{\phi}} || p_0)$ because the \mathbb{KL} divergence is not well defined between a continuous and a discrete distribution. In other words, relaxing f to \tilde{f} is not straightforward when a \mathbb{KL} divergence is involved in the objective. When using a GS relaxation, a common thing to do is to replace this \mathbb{KL} with (Jang et al., 2017; Dupont, 2018):

$$\mathbb{KL}(\bar{\alpha} || p_0) \text{ where } \bar{\alpha}_k = \frac{\alpha_k}{\sum_{i=1}^K \alpha_i} \quad (9)$$

the idea being that, for low temperatures, the GS approximates a distribution proportional to its parameter, i.e. $\bar{\alpha}$. The goal of this substitution is to still compute a \mathbb{KL} between two discrete variables, even after relaxing the distribution. This substitution is problematic, as pointed out by Maddison et al. (2017), as it does not take into account how close the GS actually is to $\bar{\alpha}$. Furthermore, this substitution of the \mathbb{KL} introduces additional issues when used with a variational autoencoder, as we will see in section 2.3. A more sensible way to relax the discrete \mathbb{KL} is to relax it to an actual continuous \mathbb{KL} as done by Maddison et al. (2017):

$$\mathbb{KL}(\tilde{q}_{\tilde{\phi}} || \tilde{q}_{\tilde{\phi}_0}) \quad (10)$$

where $\tilde{\phi}_0$ is fixed in such a way that $\tilde{q}_{\tilde{\phi}_0}$ is close to p_0 . For the GS, finding such a distribution is straightforward as a consequence of its parameter interpretability: $\tilde{q}_{\tilde{\phi}_0}$ can be chosen as a GS with parameter $\alpha_0 = p_0$.

2.3 Variational autoencoders

Variational autoencoders (VAE) (Kingma and Welling, 2014) are a central tool in machine learning for probabilistic modeling, and they have generated a huge amount of follow-up work (Higgins et al., 2017; Burda et al., 2015; Alemi et al., 2018; Loaiza-Ganem and Cunningham, 2019). They also can contain discrete latents and thus commonly use the GS. Consider the following generative model:

$$\begin{cases} Z_i \sim p_0(z) \text{ for } i = 1, 2, \dots, n \\ X_i | Z_i \sim p_\theta(x|z) \end{cases} \quad (11)$$

where p_0 is a prior distribution, θ are the parameters of a neural network and $p_\theta(x|z)$ is a distribution parameterized by the output of the neural network, whose input is z . Since performing maximum likelihood is not tractable, a lower bound $L(\theta, \phi) = \sum_{i=1}^n L_i(\theta, \phi)$ (called the ELBO) of the log likelihood is maximized instead, where:

$$\begin{aligned} L_i(\theta, \phi) &= \mathbb{E}_{q_\phi(z_i|x_i)} [\log p_\theta(x_i|z_i)] \\ &\quad - \mathbb{KL}(q_\phi(z_i|x_i) || p_0(z_i)) \end{aligned} \quad (12)$$

and $q_\phi(z_i|x_i)$ is an approximate posterior distribution, whose parameters are given by the output of a neural network parameterized by ϕ which takes x_i as input.

When p_0 is continuous it is usually chosen as a standard Gaussian and $q_\phi(z_i|x_i)$ is also chosen as a Gaussian, so that the \mathbb{KL} term in the ELBO can be computed in closed form. The reparameterization trick is then used on the first term (called the reconstruction term) in order to optimize the ELBO.

When p_0 is discrete, a continuous relaxation is used. Relaxing the reconstruction term is straightforward: the input for the neural network parameterized by θ is not a one-hot vector $z_i \in \mathcal{S}$ anymore, but a vector on the simplex, $\tilde{z}_i \in \mathcal{S}^{(K-1)}$. As mentioned in section 2.2, relaxing the \mathbb{KL} is trickier. If we use the relaxation of equation 9 the ELBO stops being a lower bound to the log likelihood, as noted by Maddison et al. (2017). We instead use the relaxation of equation 10 following Maddison et al. (2017), which is equivalent to relaxing the model to:

$$\begin{cases} \tilde{Z}_i \sim \tilde{q}_{\phi_0}(\tilde{z}) \text{ for } i = 1, 2, \dots, n \\ X_i | \tilde{Z}_i \sim p_{\theta}(x | \tilde{z}) \end{cases} \quad (13)$$

Finally, note that this relaxed \mathbb{KL} can be estimated with:

$$\mathbb{KL}(\tilde{q}_{\tilde{\phi}}(\tilde{z}_i | x_i) || \tilde{q}_{\tilde{\phi}_0}(\tilde{z}_i)) \approx \frac{1}{B} \sum_{b=1}^B \log \frac{\tilde{q}_{\tilde{\phi}}(g(\epsilon_b, \tilde{\phi}))}{\tilde{q}_{\tilde{\phi}_0}(g(\epsilon_b, \tilde{\phi}))} \quad (14)$$

which also enables estimating its gradient.

2.4 Joint VAE

For some of the models that we run in the experiments section, we modify the ELBO objective to obtain disentangled representation when the latent variables $z = (z_d, z_c)$ have both continuous and discrete components z_c and z_d , respectively. As suggested by Dupont (2018) the objective is given by:

$$\begin{aligned} L(\theta, \phi) = & \mathbb{E}_{q_{\phi}(z_d, z_c | x)} [\log p_{\theta}(x | z_d, z_c)] \\ & - \gamma |\mathbb{KL}(q_{\phi}(z_d | x) || p(z_d)) - C_{z_d}| \\ & - \gamma |\mathbb{KL}(q_{\phi}(z_c | x) || p(z_c)) - C_{z_c}| \end{aligned} \quad (15)$$

where γ , C_{z_d} and C_{z_c} are hyperparameters. The main idea is that by setting C_{z_d} and C_{z_c} to different values the model is able to encode information in the continuous and discrete components rather than ignoring the discrete component.

3 The shortcomings of the Gumbel-Softmax

The first shortcoming of the Gumbel-Softmax is its sensitivity to temperature: in order for the GS to be an adequate relaxation, it should concentrate most of its mass around the vertices of the simplex. While this concentration can be mathematically achieved at lower temperatures, in practice using low values generates two problems: (i) vanishing gradients, that result from the interplay between the softmax activation and the large values from the Gumbel noise, and (ii) numerical instabilities when estimating the \mathbb{KL} divergence of equation 14. This can be seen by noticing that having $g(\epsilon_b, \tilde{\phi})$ be a one-hot vector in equation 14 results in a division by 0, which can easily happen due to numerical underflow of the exponential function. This issue is mentioned by Maddison et al. (2017), who also propose a solution using a log transformation, resulting in what they call the ExpConcrete. As a result of this instability, the GS is usually trained with τ 's close to 0.5 (Maddison et al., 2017; Jang et al., 2017;

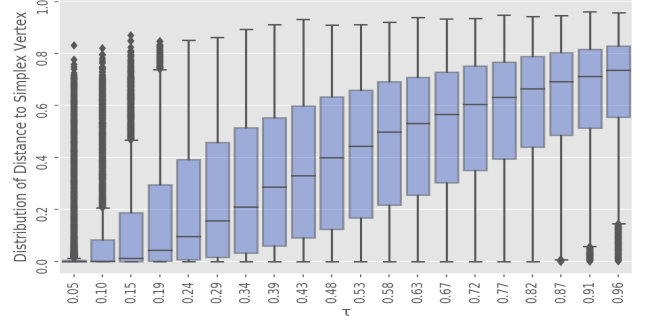


Figure 1: Distance to the nearest point on the simplex of GS samples with $\phi = (1/50, \dots, 1/50)$ with 50 categories.

Dupont, 2018), which is problematic as it makes the relaxation inadequate: samples are far from one-hot vectors and we simply have a continuous model, not a relaxation of a discrete one. Figure 1 illustrates this issue by showing the distribution of the Euclidean distance of the sample of the GS to the nearest vertex of the simplex for different temperatures. We can see that for temperatures used in practice (around 0.5), the distribution is not close to 0. As we will see in the next section, our proposed method does not suffer from these numerical instabilities as it can evaluate the \mathbb{KL} in closed form.

The GS also suffers from vanishing gradient problems at low temperatures. This problem is not only notable in the GS, but also in the ExpConcrete (see appendix A) due to its relatively heavy tails.

The second shortcoming (which is not fixed by the ExpConcrete) is that when using the GS to optimize an ELBO, a Monte Carlo estimate has to be used for the \mathbb{KL} term as in equation 14. While this estimate is not as problematic as the first shortcoming, it does introduce additional variance as compared to the continuous VAE scenario, where the \mathbb{KL} term can be computed in closed form. As we will show in section 4, our method allows for this \mathbb{KL} to be computed in closed form. The reparameterization trick thus only has to be used for the reconstruction term, resulting in lower variance estimates of the gradient of the ELBO.

4 The invertible Gaussian reparameterization family

In this section we expose our methodology for the construction of our continuous relaxation. It is inspired by the GS but it aims to address its shortcomings. The essence of the methodology is the following: first, sample noise from a Gaussian distribution. Then, transform this noise through an invertible function that

maps to $\mathcal{S}^{(K-1)}$. We choose a Gaussian parameterization as the simplest first choice because it is reparameterizable and because the \mathbb{KL} divergence between two Gaussians has closed form, but any other choice with these two properties can also be used.

The IGR distribution is parameterized by (μ, σ) , where $\mu \in \mathbb{R}^{K-1}$ and $\sigma \in (0, \infty)^{K-1}$. Gaussian noise $\epsilon = (\epsilon_1, \dots, \epsilon_{K-1}) \sim \mathcal{N}(0, I_{K-1})$ is transformed in the following way:

$$y = \mu + \text{diag}(\sigma)\epsilon \quad (16)$$

$$\tilde{z} = g(y, \tau) \quad (17)$$

where $\text{diag}(\sigma)$ is a diagonal matrix whose nonzero elements are given by σ , $g(\cdot, \tau)$ is an invertible smooth function and $\tau > 0$ is a temperature hyperparameter. The first advantage of choosing g to be an invertible function is that the density of \tilde{z} can be computed in closed form with the change of variable formula:

$$\tilde{q}_{\mu, \sigma, \tau}(\tilde{z}) = \mathcal{N}(y|\mu, \sigma) |J_g(\tilde{z}, \tau)|^{-1} \quad (18)$$

where $J_g(\cdot, \tau)$ is the Jacobian of $g(\cdot, \tau)$. The second advantage of this choice is that it allows to compute the \mathbb{KL} in closed form and the Monte Carlo estimate of equation 14 is no longer needed. The result is gradient estimators of the ELBO (or any other objective involving a \mathbb{KL} divergence) that have less variance than the GS gradients, which in turn yields more efficient optimization. Avoiding the Monte Carlo estimate also avoids the numerical difficulties of the GS, as these arise precisely from this Monte Carlo estimate. This closed form \mathbb{KL} can be verified to be given by:

$$\mathbb{KL}(\tilde{q}_{\mu, \sigma, \tau}(\tilde{z}) || \tilde{q}_{\mu_0, \sigma_0, \tau}(\tilde{z})) = \mathbb{KL}(\mathcal{N}(\mu, \sigma) || \mathcal{N}(\mu_0, \sigma_0)) \quad (19)$$

since the \mathbb{KL} divergence is invariant under the same invertible transformation. Since the parameter interpretability of the GS is lost in IGR, we cannot directly read μ_0 and σ_0 from p_0 . We thus solve the following optimization problem to obtain these parameters:

$$(\mu_0, \sigma_0) = \arg \min_{(\mu, \sigma)} \mathbb{E}_{\tilde{q}_{\mu, \sigma, \tau}}[||\tilde{z} - p_0||_2^2] \quad (20)$$

Note that having to solve this problem is a very small price to pay for losing parameter interpretability: the optimization is a very simple moment matching problem and has to be computed only once for any given prior p_0 .

4.1 Choosing $g(\cdot, \tau)$

In this section we design some invertible functions that could be used and argue the rationale behind their construction. There are two important desiderata for $g(\cdot, \tau)$: the first one is that we should be able to compute the determinant of its Jacobian efficiently, which enables tractable density evaluation. This tractability can be achieved, for example, by ensuring the Jacobian is triangular. Note that although we do not actually require evaluating the density of the relaxation when optimizing an ELBO thanks to equation 19, this is a problem-specific property and density evaluation remains desirable in general. The second is that the limit as $\tau \rightarrow 0$ of $g(y, \tau)$ is in \mathcal{S} for almost all y , meaning that as the temperature gets smaller, the distribution places most of its mass around the vertices. The two most natural choices for mapping onto the simplex are the softmax function and the stick-breaking procedure. As we explain below, these alone are not enough, and we thus modify them to make them appropriate for our purposes. The softmax has two issues: first, it maps to $\Delta^{(K-1)}$ and not $\mathcal{S}^{(K-1)}$ and second, it is not invertible. Both of these problems can be addressed with a small modification of the softmax function:

$$g(y, \tau)_k = \frac{\exp(y_k/\tau)}{\sum_{j=1}^{K-1} \exp(y_j/\tau) + \delta} \quad (21)$$

where $\delta > 0$ ensures that the function is invertible and maps to $\mathcal{S}^{(K-1)}$. Furthermore, the Jacobian of this transformation can be efficiently computed with the matrix determinant lemma. We will refer to this transformation as the softmax₊₊. Intuitively, since the Gaussian distribution has lighter tails than the Gumbel, we should expect fewer extreme samples after running Gaussian samples through a softmax₊₊ than Gumbel samples through a softmax, resulting in fewer vanishing gradients. While this effect could in principle be negated by having the Gaussian means of different coordinates very far apart, we did empirically verify that the IGR had fewer vanishing gradients than the GS (see section 5).

The other natural alternative to map from $(0, 1)^{K-1}$ onto $\mathcal{S}^{(K-1)}$ is through the stick-breaking procedure (Ferguson, 1973), which we briefly review here. Given $u \in (0, 1)^K$, the result $v = SB(u)$ of performing stick-breaking on u is given by:

$$v_k = u_k \prod_{i=1}^{k-1} (1 - v_i), \text{ for } k = 1, 2, \dots, K-1 \quad (22)$$

In addition to producing outputs in $\mathcal{S}^{(K-1)}$, this procedure has some useful properties, namely: it is invertible, its Jacobian is triangular, and it can easily

be extended to the case where $K = \infty$ (which will be useful to extend IGR to relax discrete distributions with countably infinite support). While the invertibility property might suggest that the stick-breaking procedure alone is enough to use with IGR, a temperature hyperparameter τ still needs to be introduced in such a way that as $\tau \rightarrow 0$, the resulting distribution concentrates its mass on the vertices. Unlike with the softmax_{++} , simply dividing the input by τ does not achieve this limiting behavior. Indeed, Stirn et al. (2019) transform noise from the Kumaraswamy distribution with a stick-breaking procedure to obtain a reparameterizable distribution on the simplex. Their objective is not to obtain discrete relaxations though, and they do not have a temperature hyperparameter that allows to concentrate mass on the vertices and approximate discrete distributions. The most natural way of introducing a temperature that achieves the desired limiting behavior is by linearly interpolating to the nearest vertex, resulting in a g function given by:

$$\begin{cases} w = SB(\text{sigmoid}(y)) \\ g(y, \tau) = \tau w + (1 - \tau)P_S(w) \end{cases} \quad (23)$$

where P_S is the projection onto the vertices of $\mathcal{S}^{(K-1)}$. Note that the Jacobian of this transformation is triangular. However, we found better empirical performance with the following function, which introduces the temperature using the softmax_{++} function:

$$g(y, \tau) = \text{softmax}_{++}(w/\tau) \quad (24)$$

While it might seem redundant to apply both a stick-breaking procedure and a softmax_{++} as they both map to $\mathcal{S}^{(K-1)}$, the softmax_{++} function allows to introduce τ in such a way that the distribution concentrates its mass around the vertices as $\tau \rightarrow 0$. It might then seem redundant to apply the stick-breaking procedure in the first place, we will see in the next section that applying it enables using the reparameterization trick in the countably infinite support setting.

Finally, another choice of $g(\cdot, \tau)$ could be a normalizing flow (Rezende and Mohamed, 2015; Kingma et al., 2016; Dinh et al., 2017) followed by $\text{softmax}_{++}(\cdot/\tau)$. Normalizing flows are flexible neural networks constructed in such a way that they are invertible, so that they enable us to learn g . We found planar flows (Rezende and Mohamed, 2015), which are some of the simplest normalizing flows, to be a good choice both for computational speed and because more expressive alternatives could potentially ignore the role of the temperature τ , resulting in a distribution that does not place most of its mass around the vertices.

4.2 Reparameterization trick for countably infinite distributions

Since the stick-breaking procedure can map to $\mathcal{S}^\infty = \{z \in \mathbb{R}^\infty : z_k \geq 0 \text{ and } \sum_{k=1}^\infty z_k = 1\}$, we can extend equation 24 to the setting where the discrete distribution has countably infinite support (e.g. Poisson, geometric or negative binomial distributions). In this setting, the IGR is parameterized by $\mu \in \mathbb{R}^\infty$ and $\sigma \in (0, \infty)^\infty$. Clearly backpropagating through infinitely many parameters cannot be done in a computer, but we do not have to do so as most of the parameters contribute very little to the loss. For a sample $\epsilon_1, \epsilon_2, \dots$ we only update the first K coordinates of μ and σ , where K is the number such that:

$$\sum_{k=1}^{K-1} g(y, \tau)_k \leq \rho < \sum_{k=1}^K g(y, \tau)_k \quad (25)$$

where $\rho \in (0, 1)$ is a pre-specified precision parameter and g is as in equation 24. Note that here K is now a random variable that depends on ϵ instead of being fixed as before, so that in a way the number of (effective) categories gets learned by the data. Note as well that the stick-breaking procedure is necessary to know where to cut K as it guarantees that later terms in the sequence are small, which would not happen if we only applied a softmax_{++} function.

5 Experiments

In this section, we contrast the performance of the IGR (with different choices of g) alongside that of the GS. First, in relation to section 4.2, we compare the ability of the IGR and the GS (with varying number of categories) to approximate a countably infinite distribution. We then focus on tasks that involve a \mathbb{KL} term in their objective function, since that is one of the shortcomings that we amend. We also consider a Structured Output Prediction task which does not involve a \mathbb{KL} term (and find the IGR outperforms the GS), but due to space constraints we include the results in appendix B. We consider generative models that fall into two categories. The first consists of VAEs with only discrete components where the objective is to maximize the ELBO. These experiments follow, Gu et al. (2015) and Jang et al. (2017). The second category is composed of VAEs with continuous and discrete components, as explored by Dupont (2018). Here we optimize an objective that disentangles the continuous and discrete features. The datasets we use are handwritten digits from MNIST, fashion items from FMNIST and celebrity images from CelebA. Additionally, for all the experiments, we used the log scale implementation of the GS (ExpConcrete) as in Maddison et al. (2017) since this allows us to run the models involving

the GS at lower temperatures. Throughout this section, the label IGR denotes the implementation with the softmax_{++} (equation 21) and the label IGR-SB the implementation with the stick-breaking transformation followed by a softmax_{++} (equation 24). Also for the IGR we used $\delta = 0.1$ for all the softmax_{++} functions, although we found results to not be sensitive to this hyperparameter.

Comparing any IGR variant against the GS requires selecting temperature hyperparameters for each model. To make a fair comparison, temperatures τ should be chosen carefully as they affect models differently, so they cannot just be set to the same value. In order to address this issue, we selected temperatures that resulted in similar distances to the simplex. Specifically, we selected the temperatures such that 75% of samples were at a Euclidean distance of at most 0.2 to the nearest vertex of the simplex. This choice ensures that results are comparable and that relaxed samples are actually close to their discrete counterparts. Note that properly obtaining these temperatures would require an expensive iterative procedure, where the model is trained, distance to the nearest vertex is evaluated and the temperature is then updated to then retrain the model and so on. To avoid this expensive procedure, we heuristically set temperatures to be comparable when approximating a uniform distribution, and then use those temperatures to train. We then do a sanity check after training to re-compare temperatures (as in Figure 5). Finally, for completeness, we also select the temperatures through cross validation (CV) and compare best-performing models. While these comparisons are adequate for selecting the best model, they do not take into account how good the continuous relaxations of the discrete model are. We use the notation $\text{IGR}(\tau)$ and $\text{GS}(\tau)$ to specify the used temperature τ . All implementation details are in appendix D.

5.1 Approximating a Poisson Distribution

Here we compare the ability of the IGR-SB and the GS of approximating distributions with countably infinite support. The top panels of Figure 2 show an approximation with the IGR-SB to a Poisson distribution with $\lambda = 50$, while the bottom panels show the same approximations when using a GS with different number K of discrete components. These approximations are computed by optimizing the objective in equation 20. We can see how the IGR-SB outperforms the GS, and does so without having to specify K . We show further comparisons when approximating other distributions in appendix E.

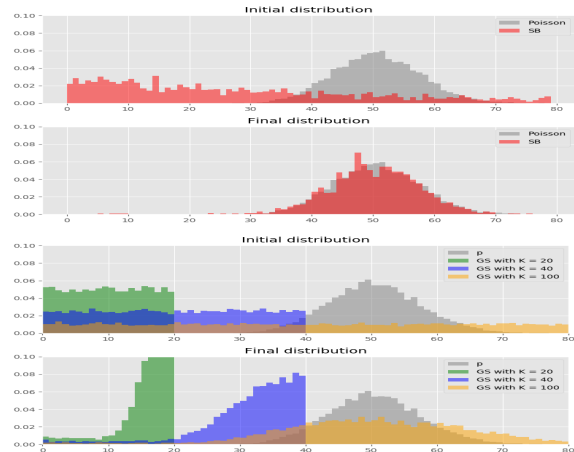


Figure 2: Approximations to a Poisson distribution for IGR-SB (second panel) and GS (fourth panel) after 1,000 training steps. Initial values of the approximations are displayed on the first and third panel, respectively.

5.2 Only Discrete Models

We trained VAEs composed of only 30 discrete variables with 10 categories. For MNIST we dynamically binarize the data and use a Bernoulli decoder, whereas for FMNIST and CelebA we use a Gaussian decoder.

Figure 3 shows the Test ELBO performance at every epoch for the IGR and GS in MNIST at different temperatures. The solid lines represent the results for the temperatures selected via CV while the dashed lines to comparable temperatures by vertex proximity. We see how the IGR outperforms its GS counterpart, both when using comparable temperatures or when selecting them through CV.

We also compare gradients of both methods in Figure 4 and observe that the number of vanishing gradients is larger for the GS. The gradient computed in this plot is the one analyzed in appendix A.

Table 1 summarizes the results for the rest of the data sets. The IGR performs best. It is worth mentioning that the execution times between the IGR and the GS were almost identical with the IGR being about 2% faster. We include further results when using normalizing flows in appendix C.

Finally, Figure 5 shows the distribution of the Euclidean distance of posterior samples to the nearest vertex, on MNIST for the IGR and GS, both for temperatures chosen by CV (high τ 's) and comparable temperatures (low τ 's). We see how the IGR and GS samples are at similar distances to the simplex vertices, showing that the IGR is genuinely outperforming the GS and not simply as an artifact of its tempera-

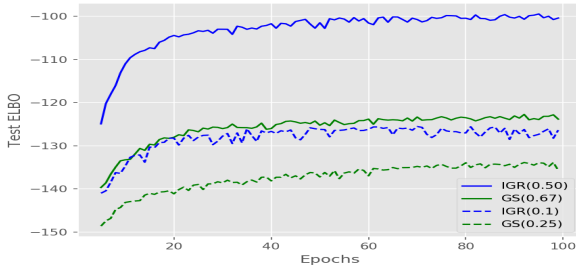


Figure 3: The mean test ELBO on dynamically binarized MNIST for 30 discrete variables with 10 categories ran 5 times. Performance of the IGR is consistently better than that of the GS. Higher is better.

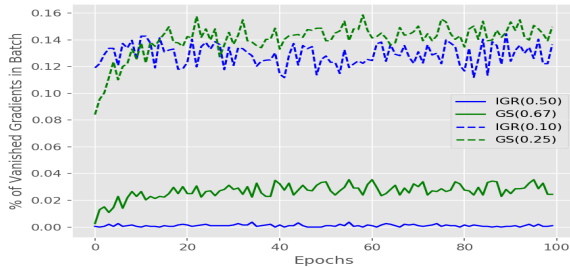


Figure 4: Percentage of gradients that vanish (numerically equal to zero) during training for the GS and IGR on the binarized MNIST for 30 discrete variables with 10 categories. Lower is better.

Models (τ)	MNIST	FMNIST	CelebA
IGR (0.50)	-1.004	-0.366	15.46
GS (0.67)	-1.219	-0.5193	13.36
IGR (0.10)	-1.264	-0.438	15.38
GS (0.25)	-1.357	-0.542	12.92

Table 1: Test ELBO (scale= 10^2) in MNIST, FMNIST (both on a dense architecture) and CelebA for IGR and GS at high temperatures (top) and low temperatures (bottom). Higher is better.

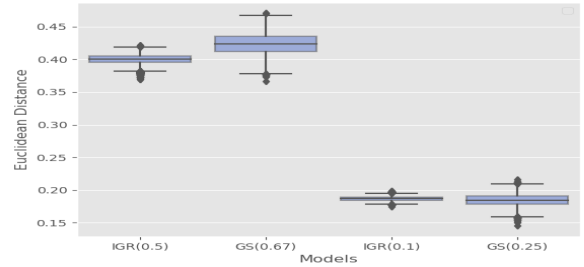


Figure 5: Distance to the simplex vertices for posterior samples of test MNIST images. For τ 's chosen by CV (left) and comparable τ 's (right).

Models (τ)	MNIST	FMNIST	CelebA
IGR (0.10)	-1.563	0.2706	9.86
GS (0.25)	-2.343	0.265	5.68

Table 2: JointVAE (scale= 10^2) across different data sets. Higher is better.

ture allowing samples to be farther away from the vertices (which could improve the ELBO while resulting in poorer relaxations).

5.3 Continuous and Discrete Models

For this setting we trained models with 10 continuous variables and a discrete component with 10 categories for the same datasets as in the previous section. We use the Joint VAE objective (equation 15). Table 2 summarizes the results. We can see that once again, the IGR outperforms the GS. We followed the hyperparameter suggestions of Dupont (2018) although their settings are not directly applicable to our context, as they used the categorical \mathbb{KL} of equation 9 as a proxy to the \mathbb{KL} . In terms of execution time gain the GS and IGR were almost indistinguishable but the IGR-SB had a 2-3 % overhead in each epoch for all datasets.

6 Conclusion

In this paper we propose IGR, a flexible discrete reparameterization as an alternative to the GS where Gaussian noise is transformed through an invertible function onto the simplex. At the cost of losing the parameter interpretability of the GS, our method recovers samples that are much closer to the simplex (and thus better relaxations) due to its increased numerical stability as well as lower variance estimates of the gradient, which results in faster convergence to better optima. Furthermore, IGR extends the reparameterization trick to discrete distributions with countably infinite support.

Acknowledgements

We thank the Simons Foundation, Sloan Foundation, McKnight Endowment Fund, NIH NINDS 5R01NS100066, NSF 1707398, and the Gatsby Charitable Foundation for support.

References

- A. Alemi, B. Poole, I. Fischer, J. Dillon, R. A. Saurous, and K. Murphy. Fixing a broken elbo. In *International Conference on Machine Learning*, pages 159–168, 2018.
- M. Balog, N. Tripuraneni, Z. Ghahramani, and A. Weller. Lost relatives of the gumbel trick. In *Proceedings of the 34th International Conference on Machine Learning-Volume 70*, pages 371–379. JMLR. org, 2017.
- L. Bottou. Stochastic gradient descent tricks. In *Neural networks: Tricks of the trade*, pages 421–436. Springer, 2012.
- Y. Burda, R. Grosse, and R. Salakhutdinov. Importance weighted autoencoders. *arXiv preprint arXiv:1509.00519*, 2015.
- L. Dinh, J. Sohl-Dickstein, and S. Bengio. Density estimation using real nvp. *ICLR*, 2017.
- E. Dupont. Learning disentangled joint continuous and discrete representations. In *Advances in Neural Information Processing Systems*, pages 710–720, 2018.
- T. S. Ferguson. A bayesian analysis of some nonparametric problems. *The annals of statistics*, pages 209–230, 1973.
- P. W. Glynn. Likelihood ratio gradient estimation for stochastic systems. *Communications of the ACM*, 33(10):75–84, 1990.
- S. Gu, S. Levine, I. Sutskever, and A. Mnih. Muprop: Unbiased backpropagation for stochastic neural networks. *arXiv preprint arXiv:1511.05176*, 2015.
- I. Higgins, L. Matthey, A. Pal, C. Burgess, X. Glorot, M. Botvinick, S. Mohamed, and A. Lerchner. beta-vae: Learning basic visual concepts with a constrained variational framework. *ICLR*, 2(5):6, 2017.
- E. Jang, S. Gu, and B. Poole. Categorical reparameterization with gumbel-softmax. *ICLR*, 2017.
- M. Johnson, D. K. Duvenaud, A. Wiltchko, R. P. Adams, and S. R. Datta. Composing graphical models with neural networks for structured representations and fast inference. In *Advances in neural information processing systems*, pages 2946–2954, 2016.
- D. P. Kingma and M. Welling. Auto-encoding variational bayes. *ICLR*, 2014.
- D. P. Kingma, T. Salimans, R. Jozefowicz, X. Chen, I. Sutskever, and M. Welling. Improved variational inference with inverse autoregressive flow. In *Advances in neural information processing systems*, pages 4743–4751, 2016.
- M. J. Kusner and J. M. Hernández-Lobato. Gans for sequences of discrete elements with the gumbel-softmax distribution. *arXiv preprint arXiv:1611.04051*, 2016.
- S. Linderman, G. Mena, H. Cooper, L. Paninski, and J. Cunningham. Reparameterizing the birkhoff polytope for variational permutation inference. In *International Conference on Artificial Intelligence and Statistics*, pages 1618–1627, 2018.
- G. Loaiza-Ganem and J. P. Cunningham. The continuous bernoulli: fixing a pervasive error in variational autoencoders. In *Advances in Neural Information Processing Systems (to appear)*, 2019.
- C. J. Maddison, A. Mnih, and Y. W. Teh. The concrete distribution: A continuous relaxation of discrete random variables. *ICLR*, 2017.
- A. Miller, N. Foti, A. D’Amour, and R. P. Adams. Reducing reparameterization gradient variance. In *Advances in Neural Information Processing Systems*, pages 3708–3718, 2017.
- T. Raiko, M. Berglund, G. Alain, and L. Dinh. Techniques for learning binary stochastic feedforward neural networks, 2014.
- D. Rezende and S. Mohamed. Variational inference with normalizing flows. In *International Conference on Machine Learning*, pages 1530–1538, 2015.
- H. Robbins and S. Monro. A stochastic approximation method. *The annals of mathematical statistics*, pages 400–407, 1951.
- A. Stirn, T. Jebara, and D. A. Knowles. A new distribution on the simplex with auto-encoding applications. 2019.
- R. J. Williams. Simple statistical gradient-following algorithms for connectionist reinforcement learning. *Machine learning*, 8(3-4):229–256, 1992.
- S. M. Xie and S. Ermon. Reparameterizable subset sampling via continuous relaxations. In *International Joint Conference on Artificial Intelligence*, 2019.

A Vanishing Gradients

Vanishing gradients are a consequence of a fundamental trade-off: lowering the temperature makes g (or the softmax) closer to a piecewise constant function which is required to adequately approximate a discrete distribution, which in turn inevitably reduces gradient information. However, intuitively the problem should be less severe for the IGR than for the GS as the noise it transforms (Gaussian) has lighter tails than the Gumbel, which we verified empirically in section 5. This vanishing gradient issue can be seen by examining the gradient of a sample \tilde{z} :

$$\begin{aligned} \nabla_{\alpha} \tilde{z}_k &= \varsigma \left(\frac{\log \alpha + \epsilon}{\tau} \right) \odot \left(e_k - \varsigma \left(\frac{\log \alpha + \epsilon}{\tau} \right) \right) \\ &\odot \left(\frac{1}{\tau \alpha} \right) \end{aligned} \quad (26)$$

where we denote the softmax function with ς and e_k is a one-hot vector with 1 in the k -th component and \odot represents element-wise multiplication. If there is a large Gumbel sample ϵ_k then this gradient vanishes since the first and second element of equation 26 become numerically zero. This issue happens even at relatively high temperatures since the Gumbel distribution samples extreme values. Implementing the Gumbel-Softmax in log space (ExpConcrete) does not solve the vanishing gradients problem since the first term in equation 27 again is numerically zero:

$$\begin{aligned} \nabla_{\alpha} \log \tilde{z}_k &= \frac{1}{\tilde{z}_k} \odot \nabla_{\alpha} \tilde{z}_k \\ &= \left(e_k - \varsigma \left(\frac{\log \alpha + \epsilon}{\tau} \right) \right) \odot \left(\frac{1}{\tau \alpha} \right) \end{aligned} \quad (27)$$

B Structured Output Prediction

In Section 5 we focused on tasks whose objective relied on computing a \mathbb{KL} divergence term. However, to isolate the improvement that comes from ameliorating the number of vanishing gradients, we ran an experiment where we wanted to minimize the Negative Log Likelihood and where no \mathbb{KL} term is involved. A benchmark task that has this characteristics is Structure Output Prediction where we predict the lower part of an image given the upper part by using binary stochastic feed-forward neural networks. This task was first proposed as a benchmark in Raiko et al. (2014) and replicated in Gu et al. (2015), Jang et al. (2017) and Maddison et al. (2017). The results of this experiment are in Table 3.

Models (τ)	NLL
IGR (0.50)	62.84
GS (0.67)	64.68
IGR (0.10)	67.26
GS (0.25)	69.28

Table 3: Structure Output Prediction test Negative Log Likelihood on binarized MNIST for different temperatures.

We observe how the IGR performs better than the GS, both for comparable and for CV-selected temperatures.

C Results with Normalizing Flows

In this section we exhibit the results of running the IGR with Normalizing Flows. These results are summarized in table 4, we used varying number of planar flow layers. We observe that IGR with normalizing flows still outperform the GS, and that simpler flows achieve very good results.

Models (τ)	FMNIST
IGR-Planar2 (0.10)	-0.3154
IGR-Planar5 (0.10)	-0.3438
IGR-Planar10 (0.10)	-0.3288
IGR (0.10)	-0.438
GS (0.25)	-0.542

Table 4: Test ELBO (scale=10²) for FMNIST. For Planar Flows with different number of layers (expressed as the last number in IGR-Planar). Higher is better.

D Architecture and hyperparameter details

In this section we describe the hyperparameters and architecture for the discrete only VAEs and for the continuous and discrete VAEs.

There were three types of neural networks used.

• Dense Architecture

- Encoder: Two fully connected dense layers of 512 units and 256 units respectively. The activations are ReLu but for the last layer linear.
- Decoder: Symmetrical to the Encoder. Two fully connected dense layers of 256 units and 512 units respectively. The activations are ReLu and linear for last layer.

- **Convolutional Architecture 1 (MNIST and FMNIST)**

- Encoder:
 - (a) 32 Conv (4×4) with stride (2×2) followed by a
 - (b) 64 Conv (4×4) with stride (2×2) followed by
 - (c) 64 Conv (4×4) with stride (2×2) followed by
 - (d) Fully connected Dense layer of 256 units.
 - * The activations are ReLu but for the last layer linear.
- Decoder:
 - (a) Fully connected Dense layer of 256 units followed by
 - (b) Fully connected Dense layer of 1024 units followed by
 - (c) 32 Conv Transpose (4×4) with stride (2×2) followed by
 - (d) 32 Conv Transpose (4×4) with stride (2×2) followed by
 - (e) 1 Conv Transpose (4×4) with stride (2×2).
 - * The activations are ReLu but for the last layer linear.

- **Convolutional Architecture 2 (CelebA)**

- Encoder:
 - (a) 32 Conv (4×4) with stride (2×2) followed by a
 - (b) 64 Conv (4×4) with stride (2×2) followed by
 - (c) 64 Conv (4×4) with stride (2×2) followed by
 - (d) 64 Conv (4×4) with stride (2×2) followed by
 - (f) Fully connected Dense layer of 256 units.
 - * The activations are ReLu but for the last layer linear.
- Decoder:
 - (a) Fully connected Dense layer of 256 units followed by
 - (b) Fully connected Dense layer of 1024 units followed by
 - (c) 64 Conv Transpose (4×4) with stride (2×2) followed by
 - (d) 32 Conv Transpose (4×4) with stride (2×2) followed by
 - (e) 32 Conv Transpose (4×4) with stride (2×2) followed by
 - (f) 3 Conv Transpose (4×4) with stride (2×2).
 - * The activations are ReLu but for the last layer linear.

D.1 Only Discrete

MNIST and FMNIST

The hyperparameters are shared across the models. The only thing that changes is the temperature which is specified by the graph.

- Batch size = 64
- Epochs = 100
- Architecture = Dense
- Learning Rate = 0.001
- Categories = 10
- Number of Discrete Variables = 30
- Image Size = (28, 28, 1)

CelebA

The hyperparameters are shared across the models. The only thing that changes is the temperature which is specified in the results of the section.

- Batch size = 64
- Epochs = 100
- Architecture = Convolutional Architecture 2
- Learning Rate = 0.001
- Categories = 10
- Number of Discrete Variables = 30
- Image Size = (68, 68, 3)

D.2 Continuous and Discrete

MNIST

The hyperparameters are shared across the models. The only thing that changes is the temperature which is specified in the results of the section. Also, only some hyperparameters apply for the IGR-SB.

- Batch size = 64.
- Epochs = 100.
- Architecture = Convolutional Architecture 1.
- Learning Rate = 0.0005.
- Number of Discrete Variables = 1.
- Categories (Discrete Latent Dimension) = 10. Valid for GS and IGR.

- Max Categories (Discrete Latent Dimension) = 50. Valid for IGR-SB only.
- Number of Continuous Variables = 1.
- Continuous Latent Dimension = 10.
- Image Size = (32, 32, 1).
- $\gamma = 30$.
- C_{z_d} = Increased linearly from 0. to 5. in 25,000 iterations.
- C_{z_c} = Increased linearly from 0. to 5. in 25,000 iterations.

FMNIST

Same as in MNIST but with the following differences

- $\gamma = 100$.
- C_{z_d} = Increased linearly from 0. to 5. in 50,000 iterations.
- C_{z_c} = Increased linearly from 0. to 10. in 50,000 iterations.

CelebA

- Batch size = 64.
- Epochs = 100.
- Architecture = Convolutional Architecture 2.
- Learning Rate = 0.0005.
- Number of Discrete Variables = 1.
- Categories (Discrete Latent Dimension) = 10. Valid for GS and IGR.
- Max Categories (Discrete Latent Dimension) = 50. Valid for IGR-SB only.
- Number of Continuous Variables = 1.
- Continuous Latent Dimension = 32.
- Image Size = (32, 32, 1).
- $\gamma = 100$.
- C_{z_d} = Increased linearly from 0. to 50. in 100,000 iterations.
- C_{z_c} = Increased linearly from 0. to 10. in 100,000 iterations.

E Approximating Discrete Distributions

Next we compare the GS and the IGR in approximating discrete distributions. We took 1,000 samples of the learned parameters of the IGR from solving equation 20.

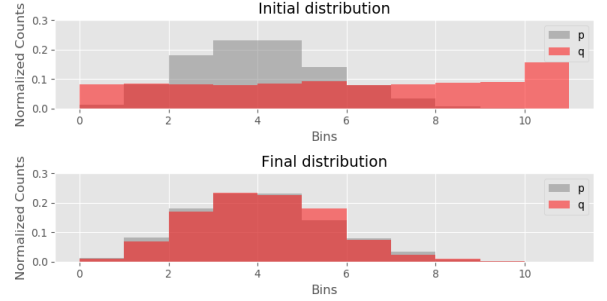


Figure 6: IGR approximation to a Binomial($N = 12, p = 0.3$)

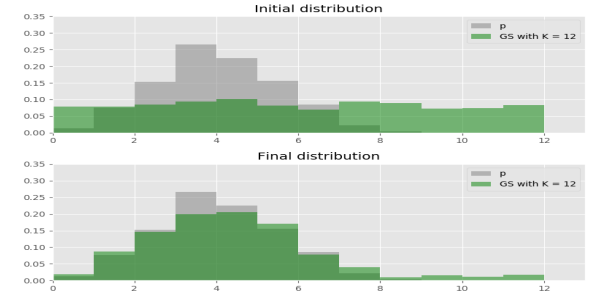


Figure 7: GS approximation to a Binomial($N = 12, p = 0.3$)

We observe how both methods approximate the Binomial adequately.

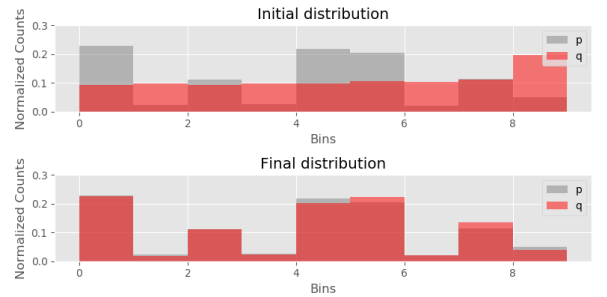


Figure 8: IGR approximation to a Discrete defined as $p = (\frac{10}{46}, \frac{1}{46}, \frac{5}{46}, \frac{1}{46}, \frac{10}{46}, \frac{10}{46}, \frac{1}{46}, \frac{6}{46}, \frac{1}{46}, \frac{1}{46})$.

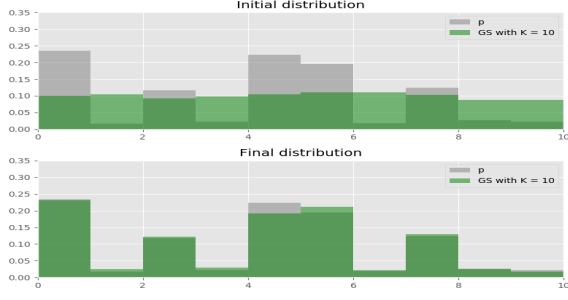


Figure 9: GS approximation to a Discrete defined as $p = (\frac{10}{46}, \frac{1}{46}, \frac{5}{46}, \frac{1}{46}, \frac{10}{46}, \frac{10}{46}, \frac{1}{46}, \frac{6}{46}, \frac{1}{46}, \frac{1}{46})$.

Also for this discrete distribution, we observe how both the GS and the IGR generate samples that are almost identical to the original distribution.

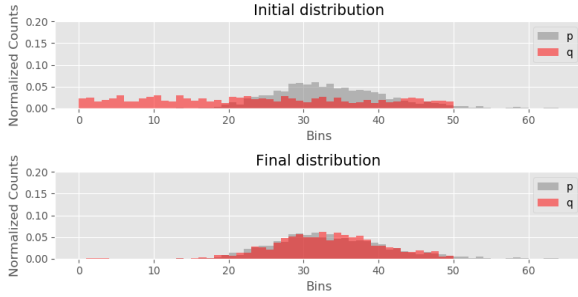


Figure 10: IGR-SB approximation to a Negative Binomial($r = 50, p = 0.6$).

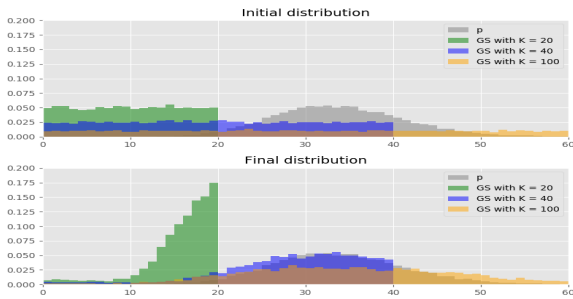


Figure 11: IGR-SB approximation to a Negative Binomial($r = 50, p = 0.6$).

Here again we see how the GS has difficulty approximating another distribution with a countably infinite support. The GS with $K = 40$ (purple) does not assign mass to the right tail whereas the GS with $K = 100$ has difficulty taking out sufficient weight from the right tail of the distribution.

F Temperature analysis

Below we show the graphs that allowed us to find the comparable temperatures between the models.

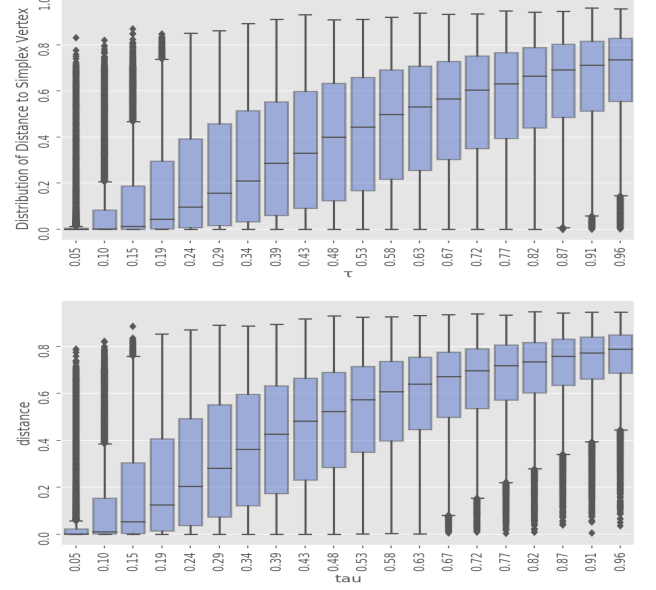


Figure 12: Distribution of the Euclidean distances to the nearest point of the simplex for the GS (top) and IGR (bottom).

As it can be seen for $\tau = 0.15$ the GS has the majority of the mass under 0.2 while the GS meets the same criteria when $\tau = 0.1$.